Measurement of Thermodynamic Parameters for Hydrophobic Mismatch 1: Self-Association of a Transmembrane Helix†

Yoshiaki Yano and Katsumi Matsuzaki*

Graduate School of Pharmaceutical Sciences, Kyoto University, Sakyo-ku, Kyoto 606-8501, Japan

Received November 7, 2005; Revised Manuscript Received January 17, 2006

ABSTRACT: Membrane partitioning and self-association of transmembrane helices are crucial thermodynamic steps for membrane protein folding, although experimental difficulties have hampered quantitative estimations of related thermodynamic parameters, especially in lipid bilayer environments. This article reports for the first time, the complete set of thermodynamic parameters (ΔG, ΔH, ΔS, and ΔC_p) for the formation of the antiparallel dimer of the inert hydrophobic model transmembrane helix X-$(AALALAA)_3$-Y (X = 7-nitro-2-1, 3-benzoxadiazol-4-yl (NBD) and Y = NH_2 (**I**) or X = Ac and Y = $NHCH_2CH_2$-S-*N*-[4-[[4-(dimethylamino)phenyl]azo]phenyl]maleimide (DABMI) (**II**)) in dimonounsaturated phosphocholine lipid bilayers with different hydrophobic thicknesses (C14−C22) at 5−55 °C, as evaluated by fluorescence resonance energy transfer from **I** to **II**. Stronger dimerization was observed in thicker membranes and at lower temperatures ($\Delta G = -9$ to -26 kJ mol^{-1}), driven by large negative ΔH values (-18 to -80 kJ mol^{-1}). Fourier transform infrared-polarized spectroscopy revealed that the peptide formed a stable transmembrane helix with an orientation angle of ∼15° in all bilayers without significant effects on lipid structures, suggesting that the depth to which the helix termini penetrate changes depending on the degree of hydrophobic mismatch. The enthalpy changes for helix−helix interactions can be well explained by the electrostatic interactions between helix macrodipoles in different dielectric environments. The new concept of dipole−dipole interaction as a basic driving force of helix dimerization will become a basis for understanding the structural and functional modifications in response to hydrophobic mismatch.

The activities of membrane proteins are significantly affected by the composition of membrane lipids (*1*−*3*). The physicochemical properties of lipid bilayers, such as rigidity and lateral pressure, are major determinants for this regulation, although more specific protein−lipid interactions are crucial in some cases. Especially, geometric matching between the hydrophobic parts of proteins and the hydrophobic thickness of surrounding lipid bilayers has been considered an important parameter for protein−lipid interactions (*4*−*7*). For example, the activity of Ca^{2+}-ATPase, which is maximal in monounsaturated phosphocholine (PC)[11] with C16 chains, is reduced to 10% of the maximal value by decreasing the chain length by only two carbons (*8*). The sorting of membrane proteins in exocytotic pathways has also been explained on the basis of hydrophobic matching. A statistical analysis found that Golgi membranes in eukaryotic cells preferentially include transmembrane helices of ∼15 amino acids, whereas thicker plasma membranes include 20 amino acids (*9*). When the hydrophobic length of a protein is longer/shorter than the hydrophobic thickness of a bilayer, namely, under positive/negative hydrophobic mismatch conditions, several adaptations to the mismatch have been proposed, such as the deformation of bilayers and/or proteins, the exclusion of proteins from bilayers, and the association of proteins in bilayers (*4*, *6*).

Instead of membrane proteins, which are intractable because of their insolubility, model transmembrane helices as the basic folding unit of helical membrane proteins have been widely used to elucidate the driving forces of membrane protein folding and the consequences of hydrophobic mismatch (*10*−*15*). This model helix approach is theoretically supported by the two-stage model of membrane protein folding (*16*, *17*), in which transmembrane protein segments are inserted into the hydrophobic core of lipid bilayers to form stable transmembrane helices (stage I), and the helices subsequently associate via helix−helix interactions to fold into the native state (stage II). To understand the thermodynamics of hydrophobic mismatch, a thermodynamic cycle that includes the transfer of helices between different membranes and the helix−helix interaction in each lipid bilayer should be considered (Figure 1). However, there are very few studies on comparisons of membrane partitioning and self-association of model transmembrane helices in different membranes. A pioneering study by Mall et al. (*12*) found, using fluorescence quenching, that the dimerization

† Supported in part by Grant-in-Aid for JSPS Fellows (155377) from the Ministry of Education, Culture, Sports, Science and Technology of Japan.

* To whom correspondence should be addressed. E-mail: katsumim@pharm.kyoto-u.ac.jp.Tel: 81-75-753-4574. Fax: 81-75-761-2698.

[1] Abbreviations: ATR, attenuated total reflection; DABMI, *N*-[4-[[4-(dimethylamino)phenyl]azo]phenyl]maleimide; diC (14:1) PC, 1,2-dimyristoleoyl-*sn*-glycero-3-phosphocholine; diC (16:1) PC, 1,2-dipalmitoleoyl-*sn*-glycero-3-phosphocholine; diC (18:1) PC, 1,2-dioleoyl-*sn*-glycero-3-phosphocholine; diC (20:1) PC; 1,2-dieicosenoyl-*sn*-glycero-3-phosphocholine; diC (22:1) PC, 1,2-dierucoyl-*sn*-glycero-3-phosphocholine; FTIR−PATR, Fourier transform infrared polarized attenuated total reflection; FRET, fluorescence resonance energy transfer; LUVs, large unilamellar vesicles; NBD, 7-nitro-2-1, 3-benzoxadiazol-4-yl; PC, phosphocholine; POPC, 1-palmitoyl-2-oleoyl-*sn*-glycero-3-phosphocholine.

10.1021/bi0522854 CCC: $33.50
Published on Web 02/17/2006

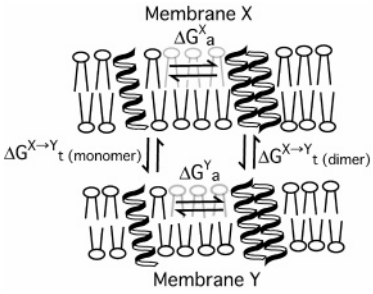

FIGURE 1: Schematic description of the thermodynamic cycle examined in this series of articles. ΔG^X_a denotes the association free energy of antiparallel dimer formation in membrane *X*, whereas $\Delta G^{X\rightarrow Y}_t$ represents the transfer free energy of the peptide from membrane *X* to membrane *Y*.

constants of polyleucine-based peptides flanked by lysine residues increased with the acyl chain length of PC. However, to fully understand the thermodynamics and the underlying mechanisms of helix−helix interactions, the measurement of not only the Gibbs free-energy change ΔG but also the corresponding enthalpy change ΔH, entropy change ΔS, and heat-capacity change ΔC_p is essential. Regarding the transfer process, no thermodynamic parameters are available to date. In this series of articles, we report for the first time the effects of hydrophobic mismatch on the complete set of thermodynamic parameters (ΔG, ΔH, ΔS, and ΔC_p) for the dimerization and intermembrane transfer of the inert hydrophobic model transmembrane helix with the symmetric sequence, X-(AALALAA)$_3$-Y (X = 7-nitro-2-1, 3-benzoxadiazol-4-yl (NBD) and Y = NH_2 (**I**) or X = Ac and Y = $NHCH_2CH_2$-S-*N*-[4-[[4-(dimethylamino)phenyl]azo]phenyl]maleimide (DABMI) (**II**)). The average hydrophobic length based on the geometric configuration of hydrophobic amino acids (*18*) is 2−3 residues shorter (27−28.5 Å), although the end-to-end length of the canonical α-helical structure is 31.5 Å. In contrast to other studies (*11*, *12*, *15*), an important feature of the helices studied here is that there are no charged or aromatic residues at the ends of the helices that would anchor the helices into membranes. To generate hydrophobic mismatch, the hydrophobic thicknesses of lipid bilayers (defined by average distances between C═O groups) were gradually changed from 20 to 34 Å using doubly monounsaturated phosphocholines with 14 to 22 acyl chain carbons: 1,2-dimyristoleoyl-*sn*-glycero-3-phosphocholine, 1,2-dipalmitoleoyl-*sn*-glycero-3-phosphocholine, 1,2-dioleoyl-*sn*-glycero-3-phosphocholine, 1,2-dieicosenoyl-*sn*-glycero-3-phosphocholine, and 1,2-dierucoyl-*sn*-glycero-3-phosphocholine (abbreviated as diC (*X*:1) PCs, *X* = 14, 16, 18, 20, and 22, respectively). Hydrophobic thicknesses of diC (*X*:1) PCs were estimated assuming a linear relationship between the thickness and the number of acyl chain carbons as follows: diC (14:1) PC, 20 Å; diC (16:1) PC, 23.5 Å; diC (18:1) PC, 27Å; diC (20:1) PC, 30.5 Å; and diC (22:1) PC, 34 Å (*19*).

In this article, the helix stability and the thermodynamic analysis of a monomer-antiparallel dimer equilibrium of the helix will be reported. The article will also describe the thermodynamic parameters associated with the intermembrane transfer of a helix as well as the accessibility of water molecules to the helix termini. We emphasize the important role of the helix macrodipole in the thermodynamics of hydrophobic mismatch.

MATERIALS AND METHODS

Materials. X-(AALALAA)$_3$-Y (X = NBD and Y = NH_2 (**I**) or X = Ac and Y = $NHCH_2CH_2$-S-DABMI (**II**)) were custom synthesized and characterized by the Peptide Institute (Minoh, Japan). The purities of the peptides (>90%) were confirmed by reverse-phase high-performance liquid chromatography, amino acid analysis, and ion-spray mass spectroscopy. All lipids were purchased from Avanti Polar Lipids (Alabaster, AL). Spectrograde chloroform and methanol were products of Nacalai Tesque (Kyoto, Japan). NMR grade 2,2,2-trifluoroethanol was purchased from Aldrich (Milwaukee, WI). The lipids and peptides were dissolved in chloroform and methanol, respectively. The lipid concentration was determined in triplicate by phosphorus analysis (*20*). The concentrations of dye-labeled peptides were determined on the basis of extinction coefficients in methanol (ϵ_{449} = 20 000 M^{-1} for **I** and ϵ_{419} = 36 900 M^{-1} for **II**), which were obtained from absorbance measurements combined with a quantitative analysis of amino acids performed in duplicate.

Fourier Transform Infrared Polarized Attenuated Total Reflection (FTIR−PATR) Spectroscopy. Oriented films of lipid/peptide were prepared by uniformly spreading a 2,2,2-trifluoroethanol solution (0.1 mL) of 50 mM lipid/1 mM peptide on a germanium ATR plate (70 × 10 × 5 mm^3) followed by gradual evaporation of the solvent. Last traces of the solvent were removed under vacuum overnight. The films were hydrated with D_2O-soaked filter paper placed over the plate for 3 h at 25 °C. FTIR−PATR measurements were carried out as described in the literature (*10*) on a BioRad FTS-3000MX spectrometer equipped with a Specac horizontal ATR attachment with a temperature controller. After the temperature was changed, the sample was equilibrated for at least 15 min before the measurements were taken. Unpolarized ATR spectra were calculated as linear combinations of polarized spectra ($0.69\Delta A_{\parallel} + \Delta A_{\perp}$) with thick-film approximations (*21*, *22*). The subscripts $_{\parallel}$ and $_{\perp}$ refer to polarized light with its electric vector parallel and perpendicular to the plane of incidence, respectively.

Preparation of Vesicles. Large unilamellar vesicles (LUVs) were prepared by an extrusion method (*23*) using a buffer containing 10 mM Tris, 150 mM NaCl, and 1mM EDTA (pH 7.4). Freezing and thawing of multilamellar vesicles containing the peptides was avoided. The concentrations of **I** (FRET donor) and **II** (FRET acceptor) in the LUV samples were precisely determined in duplicate by a least-squares fitting of absorption spectra to a linear combination of the pure absorption spectra of **I** and **II** after dissolving the peptide-incorporated vesicles with a 20-fold volume of methanol.

Determination of FRET Efficiency. FRET efficiency (E_T) or relative quantum yield ($Q_r = 1 - E_T$) was determined by the degree of NBD (donor) fluorescence quenching. Briefly, LUVs containing the donor and the acceptor were prepared as described above, and the donor fluorescence (excitation and emission at 450 and 530 nm, respectively) was compared with that of the LUVs without the acceptor in duplicate. The fluorescence measurements were made after subtracting the background scattering of vesicles in a wide range of peptide/lipid ratios from 1/10 000 to 1/200, keeping the peptide concentration in the cuvette around 0.5 μM.

E_T was calculated by

$$E_T = 1 - Q = 1 - \left(\frac{F_{DA}}{F_D}\right)\left(\frac{[D]_D^{+MeOH}}{[D]_{DA}^{+MeOH}}\right) \quad (1)$$

where F_{DA} and F_D denote the donor fluorescence intensities with and without the acceptor, respectively. $[D]_{DA}^{+MeOH}$ and $[D]_D^{+MeOH}$ express donor concentrations determined after methanol solubilization as described above. F_{DA} and F_D have been corrected for inner-filter effects (*10*) at the excitation wavelength (450 nm) because not only the donor but also the acceptor had significant absorbance in the region. The correction resulted in an increase in F of at most 2%.

Estimation of the Förster Distance. The Förster distance (R_0) for the NBD−DABMI pair was determined as described in the literature (*10*). The absorption spectrum of the acceptor and the fluorescence-emission spectrum of the donor were measured in methanol and in LUVs composed of POPC containing 0.5 mol % fluorescent probes, respectively. The flexible linker of the DABMI moiety guarantees an orientation factor of $^2/_3$. The refraction index of the medium was assumed to be 1.33.

Calculation of Association Free Energy from FRET Data. In lipid bilayers, random (spontaneous) FRET between a donor and randomly distributed acceptors as well as FRET due to donor−acceptor association contributes to the observed Q_r value.

$$Q_r = (1 - f_b)q_s + f_b q_a \quad (2)$$

The fraction of donors associated with acceptors is denoted by f_b. Relative quantum yields due to random transfer and association are expressed by q_s and q_a, respectively. The value of q_a was assumed to be 0 (see Results). The value of q_s was estimated by the theoretical analysis of Wolber and Hudson (*24*), assuming a random distribution of the acceptors in two dimensions. The required parameters in this analysis were R_0, donor−acceptor closest approach, and 2D acceptor concentration (per unit area). The surface area per lipid was assumed to be 60 Å^2 (*25*). In the case of the NBD−DABMI pair, the contribution of random FRET from trans leaflets was negligible because of the R_0 value (∼25 Å), which was smaller than the length of the helix (∼30 Å). The donor−acceptor's closest approach was evaluated to be ∼10 Å on the basis of molecular diameters. The dimer fraction (f_d) can be calculated with eq 3, assuming a monomer−dimer equilibrium and a binomial distribution of donors and acceptors in the dimer (*26*) because an oligomer without any acceptors does not contribute to FRET.

$$f_d = \frac{f_b}{1 - P_d} \quad (3)$$

P_d denotes the fraction of the donor in the donor−acceptor mixture. The association constant (K_a) and the corresponding standard Gibbs free-energy change (ΔG_a) are given by

$$\Delta G_a = -RT \ln K_a \quad (4)$$

$$K_a = \frac{[D]}{[M]^2} \quad (5)$$

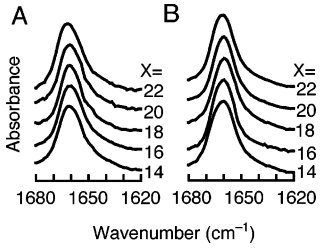

FIGURE 2: Amide I′ region spectra of D_2O-hydrated peptide/diC(X:1) PC (1/50) films at 25 °C. Unpolarized spectra that were reconstructed from polarized spectra are shown. X indicates the number of acyl chain carbons. (A) NBD-labeled peptide **(I)**. (B) DABMI-labeled peptide **(II)**.

R and T represent the gas constant and absolute temperature, respectively. [D] and [M] denote the mole fractions of the dimer and the monomer in the bilayers, respectively. The mole fraction unit is appropriate in this case, where the size of the solute (helix) is similar to that of the solvent (lipid) (*27*). Furthermore, the concentration in this unit is very close to that in the molar unit because the molecular weights of the lipids are close to 1000. Therefore, our system is free from the unit problems often discussed in evaluating thermodynamic parameters. The experiments were performed at sufficiently low peptide concentrations, expecting an ideal dilution regime.

$$[M] = (1 - f_d)\frac{2n_p}{2n_p + n_1} \quad (6)$$

$$[D] = \frac{f_d n_p}{2n_p + n_1} \quad (7)$$

$$X_p = [M] + 2[D] = \frac{2n_p}{2n_p + n_1} \quad (8)$$

The number of moles of peptides and lipids are denoted by n_p and n_l, respectively. The total-peptide mole fraction is represented by X_p. A factor of 2 is introduced to take the transmembrane nature of the peptide into consideration. In all experiments, the **I**/**II** ratio was kept around 1/0.4 because this ratio gave a sufficient fluorescence intensity of **I**, a larger signal change by dimerization, and a smaller spontaneous transfer. The association enthalpy, entropy, and heat-capacity changes were determined from temperature dependence of the association free energy (see Results).

RESULTS

FTIR−PATR. To examine the effects of hydrophobic thicknesses of bilayers on the secondary structure and orientation of the peptide, FTIR−PATR measurements were performed. The peptide/lipid molar ratio was fixed at 1/50 to obtain a sufficient signal from the peptide. At 25 °C, in all of the bilayers used, the peptide amide I′ bands showed similar narrow peaks (half-widths, ∼15 cm^{-1}) at 1661 ± 1 cm^{-1}, typical for transmembrane helical structures (*28*, *29*) irrespective of the presence of the dye at the peptide terminus (Figure 2). Similar narrow peaks were also observed at 5 and 55 °C (data not shown). The average orientation angles of the helix axis with respect to the bilayer normal calculated from the measured dichroic ratios (*21*, *22*) were also not very

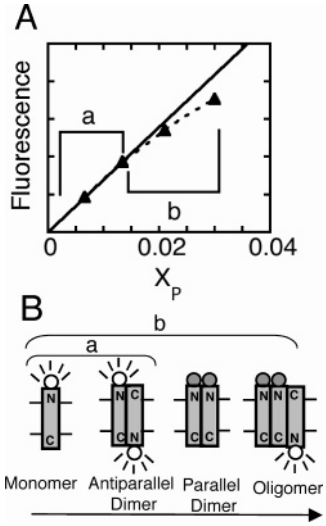

FIGURE 3: Concentration-dependent oligomerization of **I**. (A) Concentration dependence of NBD fluorescence in diC (18:1) PC at 25 °C. X_p indicates the doubled peptide mole fraction (eq 8). Self-quenching was observed in concentration range b. X_p was changed by keeping the concentration of lipid constant (50 μM). (B) Schematic representation of various oligomers. The helix is in a monomer-antiparallel dimer equilibrium in concentration range a without self-quenching. Oligomers, except for the antiparallel dimer, should involve close contact between NBD moieties, resulting in self-quenching.

sensitive to bilayer thickness, mostly in the range 10−20°, although slightly larger values were observed in diC (14:1) PC (22 ± 10°) and diC (22:1) PC (29 ± 4°) membranes at 55 °C (data not shown). Incorporation of the peptide did not have significant effects on the peak wavenumbers and dichroic ratios of the CH_2 bands of diC (*X*:1) PCs (data not shown). Overall, a stable transmembrane helical structure of the peptide was generally observed in membranes with a variety of hydrophobic thicknesses over a wide range of temperatures.

Conditions for Detection of the Antiparallel Dimer. Our previous study has suggested that the transmembrane helix $(LALAAAA)_3$ preferentially forms an antiparallel dimer at low concentrations (*10*). At higher concentrations, the formation of a parallel dimer and/or higher oligomers resulted in the self-quenching of the fluorescent probe NBD placed at the *N*-terminus of the peptide (Figure 3, footnote 3 of ref 10). The peptide $(AALALAA)_3$ used in this study should have similar properties if the major driving force of the association originates from the attraction between the helix macrodipoles. In LUVs composed of diC (14:1) PC and diC (18:1) PC, the self-quenching of **I** appeared at $X_p \sim 0.004$ and 0.014, respectively at 25 °C (Figure 4B, arrows), whereas in thicker diC (22:1) PC membranes, no self-quenching was observed in the concentration range studied. In this study, we measured the free energy of antiparallel dimer formation ΔG_a in the concentration range without self-quenching, where the peptides do not form parallel dimers or higher oligomers.

Thermodynamics for Helix-Antiparallel Dimer Formation in diC (X:1) PCs. To detect the antiparallel dimer by FRET, the fluorescence donor NBD and the acceptor DABMI were labeled at the *N*- and *C*-terminus of the peptide, respectively (**I** and **II**). In the case of the antiparallel heterodimer composed of **I** and **II**, the expected distance between the donor and the acceptor (at most 15 Å) was expected to be

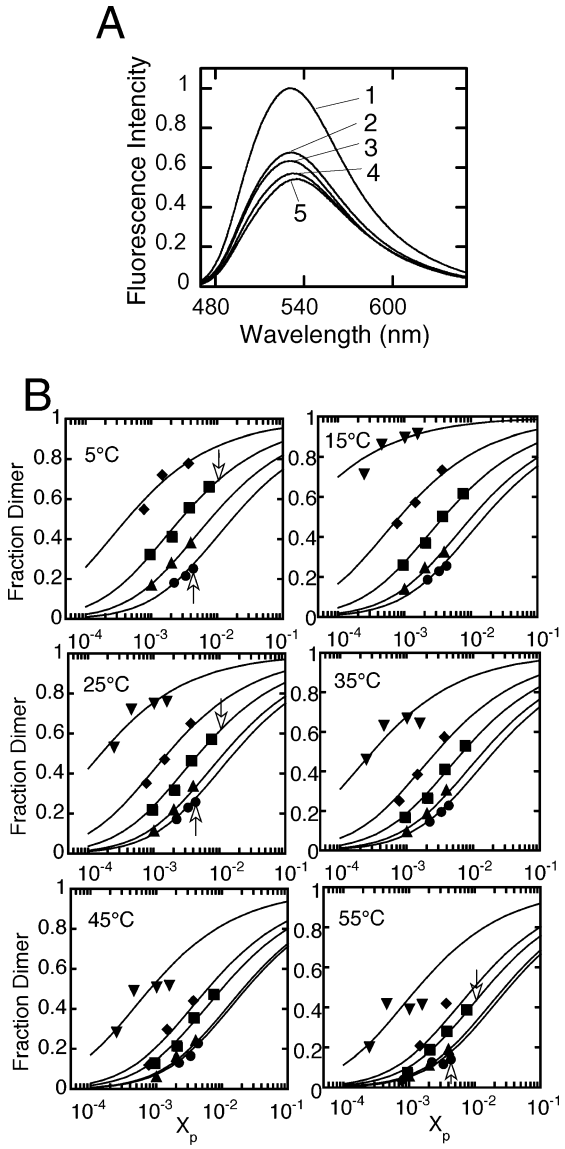

FIGURE 4: (A) Example of FRET data. Line 1 indicates the fluorescence spectrum of **I** in the absence of **II** ($X_p = 0.001$). Lines 2−5 indicate the fluorescence spectra of **I** in the presence of **II** (**I**/**II** ∼1/0.4) at X_p values of 0.001, 0.002, 0.0037, and 0.0074, respectively in diC (18:1) PC at 25 °C. (B) Monomer−dimer equilibrium of the helix in diC (*X*:1) PCs measured in 5−55 °C: $X = 14$ (●), 16 (▲), 18 (■), 20 (♦), and 22 (▼). X_p indicates the doubled-peptide mole fraction in lipids. The data was fitted with theoretical curves, assuming a monomer−dimer equilibrium (eq 9). The arrows indicate the minimal concentrations at which self-quenching of **I** occurred (5, 25, and 55 °C). In diC (22:1) PC, no self-quenching was observed up to $X_p = 0.01$.

sufficiently shorter than the R_0 value of ∼25 Å, guaranteeing a FRET efficiency higher than 95%. Furthermore, the measured R_0 values were not sensitive to temperature (25.5 and 23.1Å at 5 and 55 °C, respectively). Therefore we assumed that the fluorescence of NBD is completely quenched in the heterodimer. Spontaneous FRET originating from the random distribution of the acceptor was calculated as described in Materials and Methods. The shorter R_0 greatly decreased the degree of random transfer (at most 3% in this study) compared to the NBD−Rhodamine pair (R_0 ∼50 Å and a spontaneous transfer of >30% was observed (*10*)), enabling precise estimation of the FRET due to helix association. Figure 4A represents fluorescence spectra at

Table 1: Thermodynamic Parameters for the Formation of the Antiparallel Dimer of the Helix at 308 K

membranes	ΔG_a (kJ mol^{-1})	ΔH_a (kJ mol^{-1})	$-T\Delta S_a$ (kJ mol^{-1})	$\Delta C_{p(a)}$ (kJ K^{-1} mol^{-1})	R^2
diC (X:1) PC					
14[a]	-10.1 ± 0.1	-17.8 ± 1.5	$+7.7 \pm 1.5$	-0.4 ± 0.2	0.90
14[b]	-9.9 ± 0.1	-15.3 ± 1.9	$+5.4 \pm 1.9$		0.66
16[b]	-10.7 ± 0.4	-24.1 ± 1.0	$+13.5 \pm 1.1$		0.98
18[b]	-12.7 ± 0.4	-31.3 ± 1.0	$+18.7 \pm 1.1$		0.99
20[b]	-14.8 ± 0.5	-58.5 ± 1.5	$+43.7 \pm 1.6$		0.99
22[a]	-20.0 ± 1.2	-78.7 ± 6.5	$+58.7 \pm 6.6$	$+2.6 \pm 1.1$	0.98
22[b]	-20.8 ± 1.2	-80.0 ± 10.2	$+59.1 \pm 10.3$		0.92

[a] Estimated assuming $\Delta C_{p(a)}$ is constant in the temperature range (eq 10). [b] Estimated assuming $\Delta C_{p(a)} = 0$.

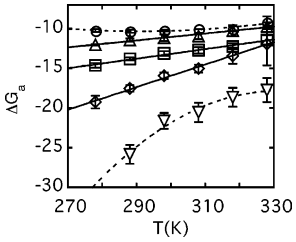

FIGURE 5: Temperature dependences of ΔG_a measured in 5−55 °C. The symbols are the same as in Figure 4B. The data was fitted by eq 10. Solid lines indicate data fitted assuming $\Delta C_{p(a)} = 0$.

various X_p values, indicating stronger FRET at higher concentrations. Figure 4B shows the dimer fraction measured in membranes with different hydrophobic thicknesses in the temperature range 5−55 °C except for diC (22:1) PC at 5 °C because the membrane is in the gel phase. The concentration dependence of dimerization well fitted the theoretical curves assuming a monomer−dimer equilibrium.

$$f_d = \frac{4K_aX_p + 1 - \sqrt{8K_aX_p + 1}}{4K_aX_p} \quad (9)$$

The ΔG_a values are summarized in Table 1. Generally, a stronger association with more negative ΔG_a values was observed in thicker membranes or at lower temperatures, ranging from -9.2 ± 0.8 kJ mol^{-1} (in diC (14:1) PC at 55 °C) to -25.8 ± 1.2 kJ mol^{-1} (in diC (22:1) PC at 15 °C). The temperature dependence of ΔG_a was analyzed assuming a constant $\Delta C_{p(a)}$ in the temperature range studied (*30*).

$$\Delta G_a = \Delta H_a + \Delta C_{p(a)}(T - T_{ref}) - T\Delta S_a - T\Delta C_{p(a)} \ln(T/T_{ref}) \quad (10)$$

T and T_{ref} represent the observed temperature and the standard-state reference temperature (308 K in this study), respectively. In cases where $X = 16$, 18, and 20, the data was adequately fitted by linear regression (Figure 5, solid lines), indicating that the changes in enthalpy and entropy upon dimerization are almost constant ($\Delta C_{p(a)} \approx 0$), whereas obvious deviations from linearity were observed for $X = 14$ and 22. The thermodynamic parameters obtained ΔH_a, $-T\Delta S_a$, and $\Delta C_{p(a)}$ at 308 K are summarized in Table 1. The association was enthalpy driven (up to -80 kJ mol^{-1} in diC (22:1) PC), and enthalpy−entropy compensation was observed. In diC (14:1) PC and diC (22:1) PC, negative and positive $\Delta C_{p(a)}$ values were obtained. We interpreted that $\Delta C_{p(a)}$ values under moderate mismatch conditions were too small to be measured precisely and that the way the helix adapts to the mismatch was essentially the same as that under more positive and negative mismatch conditions because the thermodynamic parameters changed systematically in response to the mismatch (Table 1).

DISCUSSION

Membrane systems have been proposed to adapt hydrophobic mismatch in several ways to minimize the exposure of hydrophobic parts of proteins and lipids (*4*, *6*). However, our thermodynamic data suggest that not only hydrophobic interaction but also electrostatic interactions involving helix macrodipoles play important roles in determining the type of adaptation.

Stability and Orientation of Transmembrane Helices. One possible adaptation is the distortion of helical structures. The FTIR−PATR measurements demonstrated that the transmembrane helical structure of our peptide is stable and mostly preserved in membranes with different hydrophobic thicknesses (Figure 2). Previous studies also reported that noticeable conformational changes were not observed unless the membranes were in gel phase (*11*, *31*).

Helices can also reduce hydrophobic mismatch by tilting their axes. The angle of orientation of our helix was typically ~15°. The WALP and KALP peptides also showed small orientation angles (<30°) in various PC bilayers, although a small but systematic increase in tilt angle was observed upon decreasing bilayer thickness (*11*, *32*, *33*). Maximal tilt was observed under highly positive mismatch conditions. We also observed a larger tilt (22 ± 10°) in diC (14:1) PC at 55 °C, where thermal fluctuation is maximal. Recently, the transmembrane helix of the Vpa protein was reported to change its orientation in response to hydrophobic mismatch (*34*), probably because the positively charged helix termini were always fixed at the surface of the negatively charged lipid bilayers.

Membrane deformation is another way to tolerate hydrophobic mismatch. Indeed, ^{2}H NMR studies showed that the incorporation of WALP peptides results in systematic changes in lipid bilayer thickness, although the changes are too small to fully compensate for hydrophobic mismatch (*35*, *36*). In our case, bilayer deformation was minimal. No appreciable changes in peak wavenumbers or dichroic ratios of the CH_2 stretching bands were observed in FTIR spectra. Assuming hexagonal packing between the helices and lipids, our transmembrane helix has 12 annular lipid molecules (Figure 6). Thus, the incorporation of a 2 mol % helix would affect the conformations of approximately 25% of lipids. If

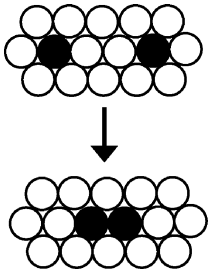

FIGURE 6: Changes in helix−helix, helix−lipid, and lipid−lipid contacts accompanying helix association assuming a hexagonal packing. Black and white circles indicate helices and lipids, respectively.

the helix had induced significant conformational changes in the surrounding lipid molecules, then such changes could have been detected by FTIR. Our spin-label study revealed that for related transmembrane helix $(LALAAAA)_3$ boundary lipids are detectable only at temperatures lower than 25 °C (*10*). Taken together, the thermodynamic data mainly reflects factors other than changes in the conformations and orientations of the helix and the lipids.

Detection of Helix Association in Lipid Bilayers by FRET. The thermodynamics of the association of helices has been mainly studied in detergent micelles. To detect oligomers in micelles, SDS−PAGE (*14*, *37*), FRET (*38*), and analytical centrifugation (*13*, *39*) techniques were successfully applied. However, there are few studies concerning the association of transmembrane helices in lipid bilayers, which faithfully reflect native environments for integral membrane proteins, because of experimental difficulties in detecting the helix association quantitatively. In addition to FRET (*10*, *40*), fluorescence quenching (*12*) and thiol-disulfide equilibria (*41*) have been utilized. Although FRET can in principle be applied to a lipid bilayer system, significant spontaneous FRET in 2D bilayers (*24*) often overwhelms the FRET signal originating from helix association, especially when the association is weak.

In this study, we carefully chose the NBD−DABMI pair and labeling positions to reduce spontaneous transfer (<3%) by decreasing the Förster distance while maintaining a high FRET efficiency (>95%) in the antiparallel dimer, enabling the precise determination of ΔG_a (error <0.4 kJ mol^{-1}). The contribution of the direct NBD−DABMI interaction to ΔG_a appears to be negligible because the ΔG_a value in diC (18:1) PC at 25 °C (-12.7 ± 0.4 kJ mol^{-1}) was almost the same as that of the peptide labeled by another FRET pair with a distant configuration X-$(LALAAA)_3$-NH_2 (X = NBD or tetramethylrhodamine) (-12.9 ± 0.8 kJ mol^{-1}) in POPC (*10*).

Helix−Helix Interaction Energetics. The formation of new helix−helix contact in lipid bilayers is associated with changes in helix−helix, helix−lipid, and lipid−lipid interactions. In a lattice-like model, *n* lipids are removed from the vicinity of the helix to bulk lipids to form *n*/2 lipid−lipid interactions (*42*, *43*).

$$\Delta G_a = \Delta G_{H-H} + \frac{n}{2}\Delta G_{L-L} - n\Delta G_{H-L} \qquad (11)$$

ΔG_{H-H}, ΔG_{L-L}, and ΔG_{H-L} denote the free energies of helix−helix, lipid−lipid, and helix−lipid interactions, respectively. Considering the difference between membranes *X* and *Y*

$$\Delta G_a^Y - \Delta G_a^X \equiv \Delta\Delta G_a^{X\to Y} = \Delta\Delta G_{H-H}^{X\to Y} + \frac{n}{2}\Delta\Delta G_{L-L}^{X\to Y} - n\Delta\Delta G_{H-L}^{X\to Y} \qquad (12)$$

Following this model, the free energy of transfer ΔG_t of the helix from membrane *X* to membrane *Y*, determined in this article, can also be described by the differences in helix−lipid and lipid−lipid interactions between membranes.

$$\Delta G_t^{X\to Y} = -\frac{k}{2}\Delta\Delta G_{L-L}^{X\to Y} + k\Delta\Delta G_{H-L}^{X\to Y} \qquad (13)$$

Here *k* lipid molecules are assumed to interact with one helix. The $\Delta\Delta G_{H-H}$ term can be extracted from measured ΔG_t and ΔG_a values.

$$\Delta\Delta G_{H-H}^{X\to Y} = \Delta\Delta G_a^{X\to Y} - \frac{n}{2}\Delta\Delta G_{L-L}^{X\to Y} + n\Delta\Delta G_{H-L}^{X\to Y} = \Delta\Delta G_a^{X\to Y} + \frac{n}{k}\Delta G_t^{X\to Y} \qquad (14)$$

Because the radii of the helix (∼5 Å) and the lipid (∼4.7 Å) on the bilayer plane are similar, hexagonal packing between the helices and the lipids can be assumed. Taking the transmembrane nature of the helix into consideration, *n* and *k* were assumed to be 4 and 12, respectively (Figure 6). The above procedure is also applicable for calculation of corresponding enthalpies and entropies. The obtained thermodynamic parameters for helix−helix interaction relative to those in diC (14:1) PC are shown in Table 2. It is suggested that helix−lipid and lipid−lipid interactions can be important factors for helix association (*4*, *6*, *12*, *44*). However, the above analysis indicates that predominant driving forces for the association originate from helix−helix interactions. For example, the $\Delta\Delta G^{14\to 22}{}_a$ (-9.9 kJ mol^{-1}) value is close to that of $\Delta\Delta G^{14\to 22}{}_{H-H}$ (-7.7 kJ mol^{-1}). The enthalpic and entropic terms were also determined by helix−helix interactions. Roughly half of $\Delta\Delta H^{14\to 22}{}_a$ (-56 kJ mol^{-1}) and $-T\Delta\Delta S^{14\to 22}{}_a$ ($+51$ kJ mol^{-1}) originated from $\Delta\Delta H^{14\to 22}{}_{H-H}$ (-32 kJ mol^{-1}) and $-T\Delta\Delta S^{14\to 22}{}_{H-H}$ ($+25$ kJ mol^{-1}), respectively.

Table 2: Thermodynamic Parameters for Helix−Helix Interactions at 308 K (relative to diC (14:1) PC)

membranes	$\Delta\Delta G^{14\to X}{}_{H-H}$ (kJ mol^{-1})	$\Delta\Delta H^{14\to X}{}_{H-H}$ (kJ mol^{-1})	$-T\Delta\Delta S^{14\to X}{}_{H-H}$ (kJ mol^{-1})
diC (*X*:1) PC			
16	-0.7 ± 0.4	-2.2 ± 1.9	$+1.6 \pm 1.8$
18	-2.5 ± 0.4	-4.3 ± 2.3	$+1.9 \pm 2.2$
20	-4.2 ± 0.5	-30.3 ± 1.6	$+26.1 \pm 1.6$
22	-7.7 ± 1.2	-32.3 ± 7.0	$+24.6 \pm 7.0$

Our results can be well explained by the hypothesis that electrostatic macrodipole interaction, which is enthalpic in nature, is the major driving force of helix−helix interactions. First, the increase in dimerization with bilayer thickness can be interpreted as enhanced electric interaction due to a lowering of the dielectric constant. Second, the facilitated parallel dimer formation in thinner membranes as evaluated by self-quenching of NBD fluorescence (Figure 4B) can be understood on the same basis: the difference in dipole-

interaction energy between antiparallel and parallel configurations is smaller in thinner membranes, where the helix termini are in more polar environments. The $\Delta\Delta H_{H-H}$ values are ascribed to dipole−dipole interaction energies, although the temperature dependence of ΔG_a is thought to contain the effects of a decrease in hydrophobic thickness at higher temperatures (a decrease of ∼0.3 Å/10 °C increase for diC (18:1) PC) (*45*). The contribution from losses of translational and rotational enthalpies ($< -3RT$) is expected to be small, especially in thicker bilayers (*46*). Dipole−dipole interaction energies (w) were calculated as

$$w(r,\theta_1,\theta_2,\phi) = -\frac{\mu_1\mu_2}{4\pi\epsilon_0\epsilon r^3}(2\cos\theta_1\cos\theta_2 - \sin\theta_1\sin\theta_2\cos\phi) \quad (15)$$

where μ, ϵ_0, ϵ, and r represent the dipole moment, dielectric constant in a vacuum, relative dielectric constant, and the distance between dipoles, respectively. The μ and r values are assumed to be 2.5×10^{-28} Cm (0.5 e × 31.5 Å) and 10 Å, respectively (*47*). In the case of an antiparallel dimer with an orientation angle of ∼15°, θ_1, θ_2, and ϕ are considered to be 105°, 255°, and 0°, respectively. Assuming that the hydrophobic thickness of diC (14:1) PC and the hydrophobic length of the helix are 20 and 28 Å, respectively, the helix termini should be positioned around phosphate group (ϵ∼45) (*48*). Given that the observed $\Delta\Delta H^{14\rightarrow20}{}_{H-H}$ and $\Delta\Delta H^{14\rightarrow22}{}_{H-H}$ values (Table 2) are totally attributable to the helix macrodipole attraction, the effective dielectric constants decrease to 9.5 and 9.1, respectively, corresponding to the burial of the helix termini around the carbonyl group (*48*). The difference in hydrophobic thickness between diC (14:1) PC (∼20 Å) and diC (20:1) PC (∼30.5 Å) is consistent with the distance between phosphate and carbonyl groups (∼5 Å × 2). However, considering the difference in hydrophobic thickness between diC (14:1) PC (∼20 Å) and diC (22:1) PC (34 Å), the helix termini should be buried in the hydrophobic core of the bilayers ($\epsilon \sim 4$) (*49*, *50*). This discrepancy suggests the existence of another factor increasing $\Delta\Delta H^{14\rightarrow22}{}_{H-H}$ in addition to helix macrodipole attraction. The observed large, positive $\Delta C_{p(a)}$ value in diC (22:1) PC implies that this originates from partial aqueous exposure of the terminal NBD and DABMI groups upon dimerization (see below). The difference (52 kJ mol^{-1}) between the calculated macrodipole attraction assuming $\epsilon = 4$ (−84 kJ mol^{-1}) and the observed $\Delta\Delta H^{14\rightarrow22}{}_{H-H}$ value (−32 kJ mol^{-1}) should originate from partial hydration of the dye moieties. Although no information is available for NBD and DABMI hydration enthalpies, they might be comparable to the value for two indole groups of +52 to +80 kJ mol^{-1} (*51*). The change in the location of the ends of the helix with changing bilayer thickness will presumably occur only for a helix without terminal anchoring residues. For example, it would not occur for a tryptophan-flanked helix (*44*).

Mall et al. reported that ΔG_a values of Leu-based peptides L16 and L22 were almost linearly dependent on the X value with a slope of −0.63 and −0.45 kJ mol^{-1} per carbon atom at 25 °C, although they discussed that a major contribution to ΔG_a comes from an interaction with lipids (*12*). These slope values are smaller than our value (∼ −1 kJ mol^{-1}), probably because electrostatic repulsion between flanking Lys residues partially masks interdipole attraction.

ΔC_p is considered to be the hallmark of the hydrophobic effect instead of ΔS. For example, globular protein unfolding at room temperature has a positive ΔC_p (*52*), whereas the partitioning of hydrophobic compounds from water to membrane generally has a negative ΔC_p (*51*). In the present study, negative and positive $\Delta C_{p(a)}$ values upon helix association were observed in thinner and thicker membranes (Table 1), implying an increase and a decrease in hydrophobic interaction, respectively. In thinner membranes, some of the terminal hydrophobic side chains exposed in the aqueous phase should come into contact with each other upon dimerization. The transfer of Ala and Leu side chains from the aqueous phase to the membrane surface yielded ΔC_p values of −0.05 and −0.38 kJ K^{-1} mol^{-1}, respectively (*30*). Thus, the observed $\Delta C_{p(a)}$ value of -0.4 ± 0.2 kJ K^{-1} mol^{-1} can be explained only by a partial dehydration of hydrophobic residues near the helix termini upon dimerization. The contribution of the side-chain dehydration to the observed ΔH_a value is expected to be small (<3 kJ mol^{-1}) (*30*). In contrast, a large, positive $\Delta C_{p(a)}$ value of 2.6 ± 1.1 kJ K^{-1} mol^{-1} was observed in diC (22:1) PC bilayers. The dimerization appeared to result in a partial aqueous exposure of the terminal NBD and DABMI groups, as inferred from the red shift of NBD fluorescence upon dimerization (e.g., an increase in dimer fraction from 0.2 to 0.6 led to a 5 nm shift; spectra not shown). Such a polarity change, which would also make a significant contribution to ΔH_a (*51*), is probably induced by the large void formed by the dimer in the interfacial region.

The increase in the entropic term $-T\Delta S_a$ up to 60 kJ mol^{-1} can originate from various sources, including changes in the hydrophobic interaction near the helix termini as discussed above, a decrease in side chain conformational entropy of up to 22 kJ mol^{-1} (*53*), and losses of the translational and rotational degrees of freedom (<8kJ mol^{-1}) (*46*).

In conclusion, our first detailed thermodynamic analysis of the formation of the antiparallel dimer of an inert model transmembrane helix in lipid bilayers strongly suggests that the dielectric environments of the helix termini change depending on the degree of hydrophobic mismatch, leading to significant changes in the strengths of helix macrodipole interactions (20−80 kJ mol^{-1}). This concept will become a basis for understanding the structural and functional modifications of integral membrane proteins in response to hydrophobic mismatch.

REFERENCES

1. Lee, A. G. (2004) How lipids affect the activities of integral membrane proteins, *Biochim. Biophys. Acta 1666*, 62−87.
2. Cornelius, F. (2001) Modulation of Na, K-ATPase and Na-ATPase activity by phospholipids and cholesterol. I. Steady-state kinetics, *Biochemistry 40*, 8842−8851.
3. Dumas, F., Tocanne, J. F., Leblanc, G., and Lebrun, M. C. (2000) Consequences of hydrophobic mismatch between lipids and melibiose permease on melibiose transport, *Biochemistry 39*, 4846−4854.
4. de Planque, M. R. R., and Killian, J. A. (2003) Protein−lipid interactions studied with designed transmembrane peptides: role of hydrophobic matching and interfacial anchoring, *Mol. Membr. Biol. 20*, 271−284.
5. Dumas, F., Lebrun, M. C., and Tocanne, J. F. (1999) Is the protein/lipid hydrophobic matching principle relevant to membrane organization and functions?, *FEBS Lett. 458*, 271−277.
6. Killian, J. A. (1998) Hydrophobic mismatch between proteins and lipids in membranes, *Biochim. Biophys. Acta 1376*, 401−415.

7. Mouritsen, O. G., and Bloom, M. (1984) Mattress model of lipid−protein interactions in membranes, *Biophys. J. 46*, 141−153.
8. Lee, A. G. (1998) How lipids interact with an intrinsic membrane protein: the case of the calcium pump, *Biochim. Biophys. Acta 1376*, 381−390.
9. Bretscher, M. S., and Munro, S. (1993) Cholesterol and the Golgi apparatus, *Science 261*, 1280−1281.
10. Yano, Y., Takemoto, T., Kobayashi, S., Yasui, H., Sakurai, H., Ohashi, W., Niwa, M., Futaki, S., Sugiura, Y., and Matsuzaki, K. (2002) Topological stability and self-association of a completely hydrophobic model transmembrane helix in lipid bilayers, *Biochemistry 41*, 3073−3080.
11. de Planque, M. R. R., Goormaghtigh, E., Greathouse, D. V., Koeppe, R. E., II, Kruijtzer, J. A., Liskamp, R. M. J., de Kruijff, B., and Killian, J. A. (2001) Sensitivity of single membrane-spanning α-helical peptides to hydrophobic mismatch with a lipid bilayer: effects on backbone structure, orientation, and extent of membrane incorporation, *Biochemistry 40*, 5000−5010.
12. Mall, S., Broadbridge, R., Sharma, R. P., East, J. M., and Lee, A. G. (2001) Self-association of model transmembrane α-helices is modulated by lipid structure, *Biochemistry 40*, 12379−12386.
13. Choma, C., Gratkowski, H., Lear, J. D., and DeGrado, W. F. (2000) Asparagine-mediated self-association of a model transmembrane helix, *Nat. Struct. Biol. 7*, 161−166.
14. Zhou, F. X., Cocco, M. J., Russ, W. P., Brunger, A. T., and Engelman, D. M. (2000) Interhelical hydrogen bonding drives strong interactions in membrane proteins, *Nat. Struct. Biol. 7*, 154−160.
15. Ren, J., Lew, S., Wang, Z., and London, E. (1997) Transmembrane orientation of hydrophobic α-helices is regulated both by the relationship of helix length to bilayer thickness and by the cholesterol concentration, *Biochemistry 36*, 10213−10220.
16. Engelman, D. M., Chen, Y., Chin, C. N., Curran, A. R., Dixon, A. M., Dupuy, A. D., Lee, A. S., Lehnert, U., Matthews, E. E., Reshetnyak, Y. K., Senes, A., and Popot, J. L. (2003) Membrane protein folding: beyond the two stage model, *FEBS Lett. 555*, 122−125.
17. Popot, J. L., and Engelman, D. M. (1990) Membrane protein folding and oligomerization: the two-stage model, *Biochemistry 29*, 4031−4037.
18. Zhang, Y.-P., Lewis, R. N., Hodges, R. S., and McElhaney, R. N. (1992) Interaction of a peptide model of a hydrophobic transmembrane α-helical segment of a membrane protein with phosphatidylcholine bilayers: differential scanning calorimetric and FTIR spectroscopic studies, *Biochemistry 31*, 11579−11588.
19. Lewis, B. A., and Engelman, D. M. (1983) Lipid bilayer thickness varies linearly with acyl chain length in fluid phosphatidylcholine vesicles, *J. Mol. Biol. 166*, 211−217.
20. Bartlett, G. R. (1959) Phosphorus assay in column chromatography, *J. Biol. Chem. 234*, 466−468.
21. Goormaghtigh, E., Raussens, V., and Ruysschaert, J. M. (1999) Attenuated total reflection infrared spectroscopy of proteins and lipids in biological membranes, *Biochim. Biophys. Acta 1422*, 105−185.
22. Matsuzaki, K., Shioyama, T., Okamura, E., Umemura, J., Takenaka, T., Takaishi, Y., Fujita, T., and Miyajima, K. (1991) A comparative study on interactions of α-aminoisobutyric acid containing antibiotic peptides, trichopolyn I and hypelcin A with phosphatidylcholine bilayers, *Biochim. Biophys. Acta 1070*, 419−428.
23. Matsuzaki, K., Murase, O., Fujii, N., and Miyajima, K. (1996) An antimicrobial peptide, magainin 2, induced rapid flip-flop of phospholipids coupled with pore formation and peptide translocation, *Biochemistry 35*, 11361−11368.
24. Wolber, P. K., and Hudson, B. S. (1979) An analytic solution to the Förster energy transfer problem in two dimensions, *Biophys. J. 28*, 197−210.
25. Wiener, M. C., and White, S. H. (1992) Structure of a fluid dioleoylphosphatidylcholine bilayer determined by joint refinement of X-ray and neutron diffraction data. III. Complete structure, *Biophys. J. 61*, 437−447.
26. Adair, B. D., and Engelman, D. M. (1994) Glycophorin A helical transmembrane domains dimerize in phospholipid bilayers: a resonance energy transfer study, *Biochemistry 33*, 5539−5544.
27. White, S. H., and Wimley, W. C. (1994) Peptides in lipid bilayers: Structural and thermodynamic basis for partitioning and folding, *Curr. Opin. Struct. Biol. 4*, 79−86.
28. Rothschild, K. J., and Clark, N. A. (1979) Anomalous amide I infrared absorption of purple membrane, *Science 204*, 311−312.
29. Haris, P. I., and Chapman, D. (1988) Fourier transform infrared spectra of the polypeptide alamethicin and a possible structural similarity with bacteriorhodopsin, *Biochim. Biophys. Acta 943*, 375−380.
30. Russell, C. J., Thorgeirsson, T. E., and Shin, Y. K. (1996) Temperature dependence of polypeptide partitioning between water and phospholipid bilayers, *Biochemistry 35*, 9526−9532.
31. Zhang, Y.-P., Lewis, R. N., Hodges, R. S., and McElhaney, R. N. (2001) Peptide models of the helical hydrophobic transmembrane segments of membrane proteins: interactions of acetyl-K_2-$(LA)_{12}$-K_2-amide with phosphatidylethanolamine bilayer membranes, *Biochemistry 40*, 474−482.
32. Ozdirekcan, S., Rijkers, D. T., Liskamp, R. M. J., and Killian, J. A. (2005) Influence of flanking residues on tilt and rotation angles of transmembrane peptides in lipid bilayers. A solid-state ^{2}H NMR study, *Biochemistry 44*, 1004−1012.
33. Strandberg, E., Ozdirekcan, S., Rijkers, D. T., van der Wel, P. C., Koeppe, R. E., II, Liskamp, R. M. J., and Killian, J. A. (2004) Tilt angles of transmembrane model peptides in oriented and nonoriented lipid bilayers as determined by ^{2}H solid-state NMR, *Biophys. J. 86*, 3709−3721.
34. Park, S. H., and Opella, S. J. (2005) Tilt angle of a trans-membrane helix is determined by hydrophobic mismatch, *J. Mol. Biol. 350*, 310−318.
35. de Planque, M. R. R., Bonev, B. B., Demmers, J. A., Greathouse, D. V., Koeppe, R. E., II, Separovic, F., Watts, A., and Killian, J. A. (2003) Interfacial anchor properties of tryptophan residues in transmembrane peptides can dominate over hydrophobic matching effects in peptide-lipid interactions, *Biochemistry 42*, 5341−5348.
36. de Planque, M. R. R., Greathouse, D. V., Koeppe, R. E., II, Schafer, H., Marsh, D., and Killian, J. A. (1998) Influence of lipid/peptide hydrophobic mismatch on the thickness of diacylphosphatidylcholine bilayers. A ^{2}H NMR and ESR study using designed transmembrane α-helical peptides and gramicidin A, *Biochemistry 37*, 9333−9345.
37. Lemmon, M. A., Flanagan, J. M., Treutlein, H. R., Zhang, J., and Engelman, D. M. (1992) Sequence specificity in the dimerization of transmembrane α-helices, *Biochemistry 31*, 12719−12725.
38. Fisher, L. E., Engelman, D. M., and Sturgis, J. N. (1999) Detergents modulate dimerization, but not helicity, of the glycophorin A transmembrane domain, *J. Mol. Biol. 293*, 639−651.
39. Fleming, K. G., Ackerman, A. L., and Engelman, D. M. (1997) The effect of point mutations on the free energy of transmembrane α-helix dimerization, *J. Mol. Biol. 272*, 266−275.
40. You, M., Li, E., Wimley, W. C., and Hristova, K. (2005) Förster resonance energy transfer in liposomes: measurements of transmembrane helix dimerization in the native bilayer environment, *Anal. Biochem. 340*, 154−164.
41. Cristian, L., Lear, J. D., and DeGrado, W. F. (2003) Use of thiol-disulfide equilibria to measure the energetics of assembly of transmembrane helices in phospholipid bilayers, *Proc. Natl. Acad. Sci. U.S.A. 100*, 14772−14777.
42. White, S. H., and Wimley, W. C. (1999) Membrane protein folding and stability: physical principles, *Annu. Rev. Biophys. Biomol. Struct. 28*, 319−365.
43. Lemmon, M. A., and Engelman, D. M. (1994) Specificity and promiscuity in membrane helix interactions, *Q. Rev. Biophys. 27*, 157−218.
44. Sparr, E., Ash, W. L., Nazarov, P. V., Rijkers, D. T., Hemminga, M. A., Tieleman, D. P., and Killian, J. A. (2005) Self-association of transmembrane α-helices in model membranes: importance of helix orientation and role of hydrophobic mismatch, *J. Biol. Chem. 280*, 39324−39331.
45. Costigan, S. C., Booth, P. J., and Templer, R. H. (2000) Estimations of lipid bilayer geometry in fluid lamellar phases, *Biochim. Biophys. Acta 1468*, 41−54.
46. Yu, Y. B., Privalov, P. L., and Hodges, R. S. (2001) Contribution of translational and rotational motions to molecular association in aqueous solution, *Biophys. J. 81*, 1632−1642.
47. Hol, W. G., van Duijnen, P. T., and Berendsen, H. J. (1978) The α-helix dipole and the properties of proteins, *Nature 273*, 443−446.
48. Mazeres, S., Schram, V., Tocanne, J. F., and Lopez, A. (1996) 7-nitrobenz-2-oxa-1,3-diazole-4-yl-labeled phospholipids in lipid membranes: differences in fluorescence behavior, *Biophys. J. 71*, 327−335.
49. Koehorst, R. B., Spruijt, R. B., Vergeldt, F. J., and Hemminga, M. A. (2004) Lipid bilayer topology of the transmembrane α-helix

of M13 Major coat protein and bilayer polarity profile by site-directed fluorescence spectroscopy, *Biophys. J. 87*, 1445−1455.
50. Handa, T., Matsuzaki, K., and Nakagaki, M. (1986) Orientations of a bifunctional molecule, 16-(9-anthroyloxy)palmitic acid, in micelles and liposomes, *J. Colloid Interface Sci. 116*, 50−58.
51. Wimley, W. C., and White, S. H. (1993) Membrane partitioning: distinguishing bilayer effects from the hydrophobic effect, *Biochemistry 32*, 6307−6312.
52. Baldwin, R. L. (1986) Temperature dependence of the hydrophobic interaction in protein folding, *Proc. Natl. Acad. Sci. U.S.A. 83*, 8069−8072.
53. Lomize, A. L., Pogozheva, I. D., and Mosberg, H. I. (2004) Quantification of helix-helix binding affinities in micelles and lipid bilayers, *Protein Sci. 13*, 2600−2612.

BI0522854